



Summary of the first neutron image data collected at the National Ignition Facility

G. P. Grim, T. N. Archuleta, R. J. Aragonéz, D. P. Atkinson, S. H. Batha, M. A. Barrios, D. E. Bower, D. K. Bradley, R. A. Buckles, D. D. Clark, D. J. Clark, J. R. Cradick, C. Danly, O. B. Drury, V. E. Fatherley, J. P. Finch, F. P. Garcia, R. A. Gallegos, N. Guler, S. M. Glenn, A. H. Hsu, N. Izumi, S. A. Jaramillo, G. A. Kyrala, S. Le Pape, E. N. Loomis, D. Mares, D. D. Martinson, T. Ma, A. J. MacKinnon, F. E. Merrill, G. L. Morgan, C. Munson, T. J. Murphy, P. J. Polk, D. W. Schmidt, T. Tommasini, I. L. Tregillis, A. C. Valdez, P. L. Volegov, T. F. Wang, C. H. Wilde, M. D. Wilke, D. C. Wilson, J. M. Dzenitis, B. Felker, D. N. Fittinghoff, M. Frank, S. N. Liddick, M. J. Moran, G. P. Roberson, P. B. Weiss, M. I. Kauffman, S. S. Lutz, R. M. Malone, A. Traille

November 7, 2011

Inertial Fusion Sciences and Applications
Bordeaux, France

September 12, 2011 through September 16, 2011

Disclaimer

This document was prepared as an account of work sponsored by an agency of the United States government. Neither the United States government nor Lawrence Livermore National Security, LLC, nor any of their employees makes any warranty, expressed or implied, or assumes any legal liability or responsibility for the accuracy, completeness, or usefulness of any information, apparatus, product, or process disclosed, or represents that its use would not infringe privately owned rights. Reference herein to any specific commercial product, process, or service by trade name, trademark, manufacturer, or otherwise does not necessarily constitute or imply its endorsement, recommendation, or favoring by the United States government or Lawrence Livermore National Security, LLC. The views and opinions of authors expressed herein do not necessarily state or reflect those of the United States government or Lawrence Livermore National Security, LLC, and shall not be used for advertising or product endorsement purposes.

Summary of the first neutron image data collected at the national ignition facility

Gary P. Grim^{1,a}, Thomas N. Archuleta¹, Robert J Aragonese¹, Dennis P Atkinson², Steven H Batha¹, Maria A Barrios², Dan E Bower², David K. Bradley², Robert A Buckles³, David D Clark¹, Deborah J Clark¹, Deborah J Clark¹, Jerry R Cradick³, Chris Danly¹, Owen B Drury², Valerie E Fatherley¹, Joshua P Finch⁵, Felix P Garcia¹, Robert A Gallegos¹, Nevzat Guler¹, Steven M. Glenn², Albert H. Hsu¹, Nobuhiko Izumi, Steven A Jaramillo¹, George A. Kyrala¹, Sebastien Le Pape², Eric N Loomis¹, Danielle Mares¹, Drew D Martinson¹, Tammy Ma², Andrew J. Mackinnon, Frank E Merrill¹, George L Morgan¹, Carter Munson¹, Thomas J Murphy¹, Thomas J Murphy¹, Paul J Polk¹, Derek W Schmidt¹, Riccardo Tommasini², Ian L Tregillis¹, Adelaida C Valdez¹, Petr L Volegov¹, Tai-Sen F Wang¹, Carl H Wilde¹, Mark D Wilke¹, Douglas C. Wilson¹, John M Dzenitis², Brian Felker², David N Fittinghoff², Matthias Frank², Sean N Liddick², Michael J Moran², George P Roberson², Paul Weiss², Morris I Kauffman⁴, Steve S Lutz³, Robert M Malone⁴, and Albert Traille³

¹ Los Alamos National Laboratory, Los Alamos, NM 87545, USA

² Lawrence Livermore National Laboratory, Livermore, CA 94550 USA

³ National Security Technologies, Livermore Operations, Livermore CA 94550 USA

⁴ National Security Technologies, Los Alamos Operations, Los Alamos, NM 87544 USA

⁵ National Security Technologies, Special Technology Laboratory, Santa Barbara, CA 93111 USA

⁶ Global Nuclear Fuel, Wilmington, North Carolina 28402, USA

Abstract. A summary of data and results from the first neutron images produced by the National Ignition Facility (NIF), Lawrence Livermore National Laboratory, Livermore, CA, USA are presented. An overview of the neutron imaging technique is presented, as well as a synopsis of the data collected and measurements made to date. Data from directly driven, DT filled microballoons, as well as, indirectly driven, cryogenically layered ignition experiments are presented. The data presented show that the primary cores from directly driven implosions are approximately twice as large, $64 \pm 3 \mu\text{m}$, as indirect cores 25 ± 4 and $29 \pm 4 \mu\text{m}$ and more asymmetric, $P2/P0 = 47\%$ vs. -14% and 7% . Further, comparison with the size and shape of X-ray image data on the same implosions show good agreement, indicating X-ray emission is dominated by the hot regions of the implosion. This work was performed for the U.S. Department of Energy, National Nuclear Security Administration and by the National Ignition Campaign partners; Lawrence Livermore National Laboratory (LLNL), University of Rochester -Laboratory for Laser Energetics (LLE), General Atomics(GA), Los Alamos National Laboratory (LANL), Sandia National Laboratory (SNL). Other contributors include Lawrence Berkeley National Laboratory (LBNL), Massachusetts Institute of Technology (MIT), Atomic Weapons Establishment (AWE), England, and Commissariat à l'Énergie Atomique (CEA), France. LA-UR 11-06250

1 Introduction

The National Ignition Facility has begun the quest to systematically determine the conditions necessary to ablatively drive a cryogenically layered DT filled capsule to the pressures and temperatures necessary to induce thermonuclear burn, with the goal of obtaining energetic break-even. To achieve the requisite drive conditions, it is necessary to carry out a series of “tuning” experiments where the empirical relationship between key fuel assembly properties, such as size and shape, can be correlated with the laser drive parameters, such as pointing within the hohlraum, power, power balance, pulse timing, etc. Images of where fusion neutrons are produced and scattered within the highly compressed fuel assembly provides key information on the

efficiency of the implosion. This information, when combined with other data, such as ion temperature, yield, bang-time, etc, can be used to provide a detailed picture of the burning plasma and the material surrounding it, allowing measurements of fuel volume, areal density, pressure, adiabat, etc. In this work, the first neutron image data produced by the NIF neutron imaging diagnostic is presented. In section 2 a brief synopsis of the method is provided, followed by a summary of the data collected to date in section 3, as well as a comparison with X-ray image data in section 3.3. Section 4 summarizes the results.

2 The NIF Neutron Imager

Fig. 1 illustrates how neutron imaging works and what information it can provide. As the core of the fuel in DT im-

^a e-mail: gpgrim@lanl.gov

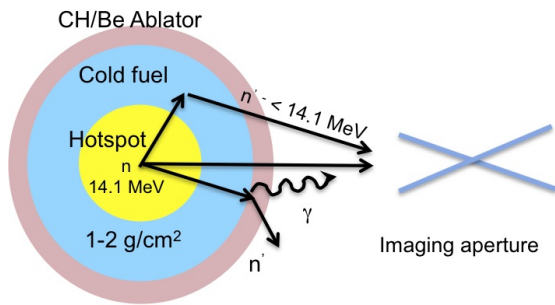


Fig. 1. Description of the physical processes contributing to neutron imaging.

plosions reaches temperatures and densities where a large number of DT fusions occur, a corresponding flux of 14.1 MeV neutrons will be produced and stream from the 50–150 μ diameter, hot-spot. As these neutrons leave the capsule, they will pass through colder, denser fuel that is not participating in the burn and a significant fraction will undergo subsequent nuclear scatters. These scatters result in a spectrum of neutron kinetic energies that extend from 14.1 MeV, down thermal energies. The fraction of neutrons found in the energy band from 10–12 MeV can be related to the areal density of the cold dense fuel, and therefore an excellent measure of the size and shape of the dense mass surrounding the hot spot.

Neutron imaging of inertial confinement fusion implosions is a well established diagnostic technique[1–5]. The diagnostic principle, is based on aperture imaging methods regularly used in optics. In inertial confinement fusion experiments, source sizes are typically 100 μm in diameter. To provide images with sufficient resolving capability, apertures with 10 μm are required. Since the mean-free-path of fast neutrons in suitable aperture materials is greater than 3 cm, aperture bodies are typically at least 10 cm in length. The obliquity of a 10 μm hole through a 10 cm body requires object distances in excess of 10 cm, with sufficient margin to allow for target misalignment. Further, fast neutrons are efficiently detected (imaged) in organic scintillator materials, which have a proton recoil lengths, and therefore imaging resolution ~ 1 mm. To reduce the contribution of the imaging detector resolution from millimeters to micrometers, a magnification approaching 100 is required, and therefore the detector must be located at distances greater than 10 m from the source. The data collected by the NIF neutron imaging diagnostic were collected in the equatorial plane of the the NIF coordinate system, using a 20 cm long gold and tungsten aperture body located at a pinhole imaging object distance of 32.5 cm from the target. The neutrons were detected in a 170 mm x 170 mm x 5 cm volume of coherently arrayed, 250 μm diameter, BCF99-55 scintillating fibers positioned 2800 cm from the target. Light from this volume was collected in two digital recording system, electro-optically gated on neutron flight times corresponding to energy gates of 10–12 MeV and 13–17 MeV. The details of the diagnostic development are published in a number

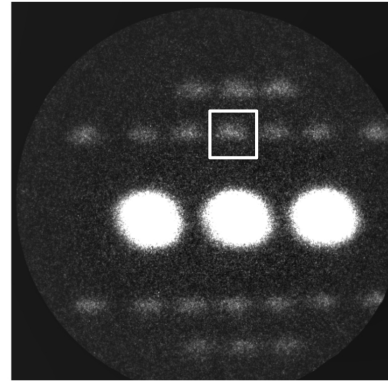


Fig. 2. First data from the NIF neutron imaging diagnostic. Shown is the background and detector corrected array of aperture images of the primary neutron flux produced by the implosion of a directly driven, 1.4 mm, SiO₂ capsule filled with 10 atm of DT.

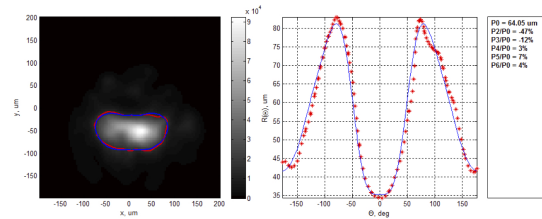


Fig. 3. Reconstructed pinhole image from the aperture shown within the box drawn in Fig. 2. The red curve on the image is the 17% of peak intensity contour, while the blue curve is the fit to the 17% contour expanding in Legendre polynomial series. The fit yields a $P0 = 64 \pm 3 \mu\text{m}$, and a $P2/P0$ of $-47 \pm 4 \%$.

of papers[6–8] and the details of this system are described in a separate submission by Fittinghoff et al.[9].

3 Neutron Imaging Data

3.1 Direct Drive Implosions

Fig. 2 shows the first image data collected from the NIF neutron imaging diagnostic. The images were produced by fusion neutrons from a directly driven, 1.5 mm diameter, 4 μm thick glass capsule filled with 10 atm of equimolar DT. The laser pulse duration was ~ 2.0 ns, irradiating the glass shell with 125 kJ of 351 nm energy. The images were corrected for detector and background systematics. The array of images reflect the aperture assembly, which is a grand array[10] of 20 pinholes surrounding a row of three neutron penumbral apertures[1,2]. The axis of each aperture within the array, excluding of the outer four apertures in the two rows of 7 pinholes, was designed to converge at a point 26.5 cm in front of the body. The pinhole cross sections are equilateral triangles of varying height within the assembly. The projected aperture surfaces circumscribe a 200 μm circle 26.5 cm from the front of the assembly. For these images, the aperture was positioned 32.5 cm from the imploded target, so each aperture centerline points to a different location at the target plane. Due to the finite aperture field-of-view, the resultant variation of the signal with

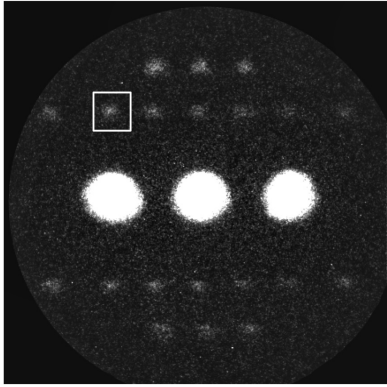


Fig. 4. First data from the NIF neutron imaging diagnostic. Shown is the background and detector corrected array of aperture images of the primary neutron flux produced by the implosion of a directly driven, 1.4 mm, SiO₂ capsule filled with 10 atm of DT.

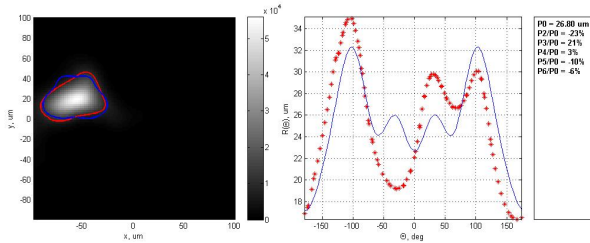


Fig. 5. Reconstructed pinhole image from the first layered implosion data collected by the NIF neutron imaging diagnostic. The image was reconstructed from the data within the box in Fig. 4. The target was a cryogenically layered CH capsule filled with 15% H, 20% D and 65% T and driven by 1.3 MJ of 351 nm energy.

pinhole pointing may be used to determine the location of the source, a necessary condition for image reconstruction. The box drawn in Fig. 2 illustrates the measured pointing of the pinhole most closely aligned to the source. The image is then cropped around this center location, and reconstructed using an Estimation Maximization Maximum Likelihood algorithm[11]. The results of this reconstruction are shown in Fig. 3. The shape of the core, as described by coefficients of a Legendre polynomial fit of the radius versus angle at the 17% of peak signal contour are: $P_0 = 64 \pm 3 \mu\text{m}$ and $P_2/P_0 = 47 \pm 4 \%$. The significant asymmetry of the implosion is due to the difficulty in the polar distribution of the laser beams to provide significant drive at the waist of the target due to the high glancing angle. In spite of this, the data show good agreement with X-ray imaging data, as well as, post-shot simulations of the size and shape of the fuel assembly, as described by Wilson et al.[12].

3.2 Images from cryogenically layered targets

Since commissioning, the neutron imaging diagnostic has participated in eight cryogenically layered DT and HTD implosion experiments. Fig. 4 shows the first image data from these implosion, shot N110603-001-999, an HTD filled

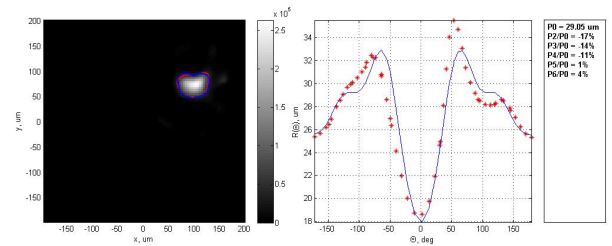


Fig. 6. Reconstructed pinhole image data of primary neutrons from shot N110608-001-999. Shot N110608 was a cryogenically layered equimolar DT filled capsule shot at 1.3 MJ of 351 nm energy. The result of the fit gives: $P_0 = 29 \pm 4 \mu\text{m}$, and $P_2/P_0 = -17 \pm 4 \%$.

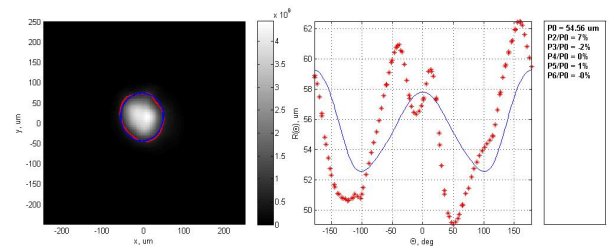


Fig. 7. First reconstructed penumbral aperture image of scattered neutrons. The shows the fluence of 10-12 MeV neutrons produced in shot N110608-002-999. The fit results are: $P_0 = 54.6 \pm 6 \mu\text{m}$ and $P_2/P_0 = 7 \pm 3 \%$.

plastic capsule designed with a 57μ thick CH ablator. The deuterium fraction for this shot was 20%, while the fractions of the H (15%) and T (85%) maintained an average atomic mass number of 2.5. The capsule was driven with 1.3 MJ of 351 nm radiation at a peak power near 420 TW. The data shown are the detector and systematics corrected images from the primary neutron flux in the 13 to 17 MeV energy band. Using the same methods described above, the image within the box shown in Fig. 5 was reconstructed at the 17% of peak signal contour, and was fit for shape information. The resulting Legendre mode description of the low mode shape was: $P_0 = 25 \pm 3 \mu\text{m}$, and $P_2/P_0 = -24 \pm 3 \%$. The error bar quoted is a combined error bar including the systematic uncertainty in the fit. This was determined by the fit uncertainties and a replicate trials study using the current noise model of the image system. The neutron yield and downscattered ratio of this shot was $6.45\text{E}+13 \pm 1.53\text{E}+12$, and $4.4 \pm 0.3 \%$, therefore the number neutrons in the 10-12 MeV band was below the sensitivity threshold ($\sim 2\text{E}+13$) for pinhole imaging.

Figs. 6 and 7 shows the reconstructed primary and 10-12 MeV scattered images from shot N110608-002-999, which produced in a primary neutron yield of $1.9\text{E}+14 \pm 4.4\text{E}+13$ and a downscattered neutron flux ratio (DSR) between the 10-12 MeV and 13-17 MeV bands of $4.4 \pm 0.2 \%$. At these yields and DSR levels, a penumbral downscattered image reconstruction may be performed. The capsule used in this implosion was similar to shot N110603-001-999, but filled with equimolar DT. The resulting P_0 and P_2/P_0 ratio for the primary and downscattered reconstructions are: $P_{0_{prim}} = 29 \pm 4 \mu\text{m}$, $P_{2/P_0_{prim}} = -17 \pm 4 \%$, and

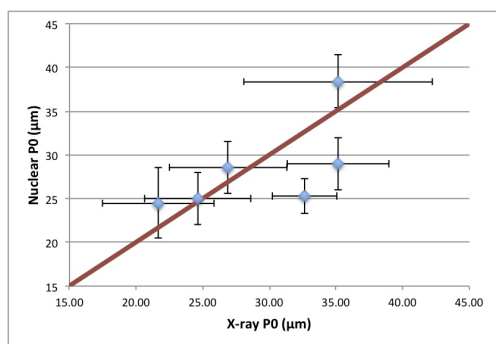


Fig. 8. Neutron P0 vs. X-ray P0 from cryogenically layered DT and THD implosions at the NIF. The data show good agreement between the size of the nuclear and X-ray images supporting the conclusion that the X-ray images are produced in the hot core of the implosion.

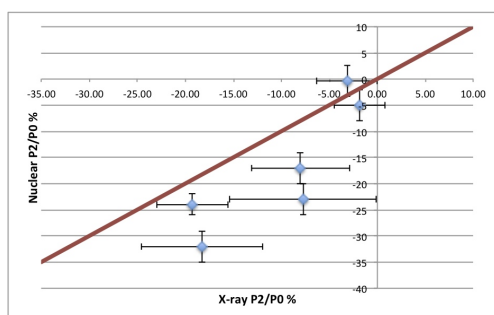


Fig. 9. Neutron P2/P0 vs. X-ray P2/P0 from cryogenically layered DT and THD implosions at the NIF. The data show good trend agreement, though nuclear hot spot appears to be slightly more asymmetric than the X-ray volume.

$P0_{sec} = 54 \pm 7 \mu\text{m}$, $P2/P0_{sec} = -7 \pm 3\%$. The downscattered ratio expected from this geometry, and under the assumption of an isobaric configuration, concentric registration of the image centroids, and fuel mass conservation, is about 4%, in good agreement between this image data and other measurements of the neutron fluence from the implosion.

3.3 Comparison with x-ray image data

Figs. 8 and 9 shows a comparison of the primary neutron image and X-ray images collected at peak burn. The data were produced in the series of layered cryogenic implosions that occurred during the summer of 2011. These two data sets are collected from image systems mounted on the equatorial plane relative to the hohlraum axis, but separated by 123° in azimuthal angle, around the axis. The data show good agreement between the two diagnostic techniques, even though the images are formed from different physical phenomena. Since neutron images show where the fuel assembly is hot, resulting in nuclear reactivity, the resultant similarity between the size and shape of the X-ray data, indicate that the X-rays are produced in the same hot volume, and that the 9-11 KeV energy X-ray production is dominated by temperature and not density.

4 Summary

During the past year, the NIF neutron imaging system has been implemented and operationally qualified. During this period, the system has collected images of polar direct drive implosions of DT filled micro balloons, as well as indirectly driven layered cryogenic implosions of HTD and DT filled plastic capsules. Data from these experiments have been analyzed for fuel assembly size and shape data. For direct drive implosions, the primary core size has been measured to be approximately two times larger than for indirect drive implosions, and substantially more asymmetric. Further the NIF neutron imager has also collected primary and scattered neutron images of cryogenically layered HTD and DT filled CH shells, with the scattered neutron images representing an experimental first. The size and shape of the neutron hot-spot shows quantitative agreement with the x-ray image data, and indicating that X-ray emission appears to be dominated by the hot core of the implosion.

References

1. D. Ress, R.A. Lerche, R.J. Ellis, S.M. Lane, K.A. Nugent, *Rev. Sci. Instrum.* **59**, 1694 (1988)
2. J.P. Garçonnet, O. Delage, D. Schirmann, A. Bertin, G. Grenier, B. Guilpar, A. Rouyer, *Lasers and Part. Beams* **12**, 563 (1994)
3. L. Disdier, A. Rouyer, D. Wilson, A. Fedotoff, C. Stoeckl, J.L. Bourgade, V.Y. Glebov, J.P. Garçonnet, W. Seka, *Nucl. Instrum. Meth. A* **489**, 496 (2002)
4. C.R. Christensen, C. Barnes, G. Morgan, M. Wilke, D.C. Wilson, *Rev. Sci. Instrum.* **74**, 2690 (2003)
5. G.P. Grim, G.L. Morgan, M.D. Wilke, P.L. Gobby, C.R. Christensen, D.C. Wilson, *Rev. Sci. Instrum.* **75**, 3572 (2004)
6. G.P. Grim, et al., *Jour. de Phys. IV* **133**, 913 (2006)
7. C.H. Wilde, D.D. Clark, V.E. Fatherley, G.P. Grim, S.A. Jaramillo, A.J. Montoya, G.L. Morgan, J.A. Oertel, T.A. Ortiz, J.R. Payton et al. (2007)
8. M.D. Wilke, S.H. Batha, P.A. Bradley, R.D. Day, D.D. Clark, V.E. Fatherley, J.P. Finch, R.A. Gallegos, F.P. Garcia, G.P. Grim et al., *Rev. Sci. Instrum.* **79**, 10E529 (2008)
9. D.N. Fittinghoff, D.P. Atkinson, D.E. Bower, O.B. Drury, J.M. Dzenitis, B. Felker, M. Frank, S.N. Liddick, M.J. Moran, G.P. Roberson et al., *European Journal of Physics* (Submitted to the current conference proceedings)
10. R.F. Wagner, D.G. Brown, C.E. Metz, *Proceedings of the SPIE* **314**, 72 (1981)
11. V.I. Gelfgat, E. Kosarev, E. Podolyak, *Computer Physics Communications* **74**, 335 (1993)
12. D.C. Wilson, T.N. Arhucleta, R.J. Aragonez, D.P. Atkinson, M.A. Barrios, S.H. Batha, D.E. Bower, D.K. Bradley, R.A. Buckles, D.D. Clark et al., *European Journal of Physics* (Submitted to the current conference proceedings)